

GT2011-46448

THE INFLUENCE OF TURBINE STATOR WELL COOLANT FLOW RATE AND
 PASSAGE CONFIGURATION ON COOLING EFFECTIVENESS

D. D. Coren*, N. R. Atkins[†],
 C. A. Long, D. Eastwood

Thermo-Fluid Mechanics Research Centre
 University of Sussex
 Brighton, BN1 9QT, UK

P. R. N. Childs

Dept. of Mechanical Engineering
 Imperial College London
 South Kensington
 London, SW7 2AZ, UK

A. Guijarro-Valencia,

J. A. Dixon
 Thermal Systems
 Rolls-Royce plc
 Derby, UK

ABSTRACT

Market competitiveness for aero engine power plant dictates that improvements in engine performance and reliability are guaranteed *a priori* by manufacturers. The requirement to accurately predict the life of engine components makes exacting demands of the internal air system, which must provide effective cooling over the engine duty cycle with the minimum consumption of compressor section air. Tests have been conducted at the University of Sussex using a turbine test facility which comprises a two stage turbine with an individual stage pressure ratio of 1.7:1. Main annulus air is supplied by an adapted Rolls-Royce Dart compressor at up to 440 K and 4.8 kg s⁻¹. Cooling flow rates ranging from 0.71 to 1.46 $C_{w, ent}$, a disc entrainment parameter, have been used to allow ingress or egress dominated stator well flow conditions. The mechanical design of the test section allows internal cooling geometry to be rapidly re-configured, allowing the effect of jet momentum and coolant trajectory to be investigated. An important facet to this investigation is the use of CFD to model and analyse the flow structures associated with the cavity conditions tested, as well as to inform the design of cooling path geometry. This paper reports on the effectiveness of stator well coolant flow rate and delivery configurations using experimental data and also CFD analysis to better quantify the effect of stator well flow distribution on component temperatures.

NOMENCLATURE

a	Disc inner radius [m]
A	Cross sectional area
b	In-cavity disc outer radius [m]
C_D	Discharge coefficient
C_p	Specific heat at constant pressure [J kgK ⁻¹]
d	Inner Diameter [m]
D	Outer diameter [m]
N	Turbine speed [rpm]
m	Mass flow rate [kg s ⁻¹]

P	Static pressure [Pa]
P_0	Total pressure [Pa]
r	Local radius [m]
R	Universal gas constant
s	Axial rotor-stator spacing [m]
T	Static temperature [K]
T_0	Total temperature [K]
v_ϕ	Tangential velocity component [ms ⁻¹]
v_z	Axial velocity component [ms ⁻¹]
ω	Rotational speed [rad s ⁻¹]
ρ	Density [kg m ⁻³]
μ	Dynamic viscosity [Pa s]

Dimensionless

C_w	Non-dimensional throughflow, $m b\mu^{-1}$
G	Cavity aspect ratio, sb^{-1}
Re_ϕ	Rotational Reynolds number, $\rho\omega b^2\mu^{-1}$
Re_z	Annular seal Reynolds number, $\rho v_z(D-d)\mu^{-1}$
β	Swirl ratio, $v_\phi r\omega^{-1}$
λ_T	Flow parameter, $C_w Re_\phi^{-0.8}$

Subscripts

0	Free disc flow value
1	Station upstream of Stator 1, <i>main annulus</i>
2	Station upstream of Rotor 1, <i>main annulus</i>
3	Station upstream of Stator 2, <i>main annulus</i>
4	Station upstream of Rotor 2, <i>main annulus</i>
<i>cold</i>	Cold Reference value
<i>coolant</i>	Coolant condition
<i>ent</i>	Disc entrainment flow
<i>hot</i>	Hot reference value
<i>inlet</i>	Inlet condition
<i>metal</i>	Metal condition
<i>s</i>	Superposed flow value

Abbreviations

CFD	Computational Fluid Dynamics
-----	------------------------------

*Correspondence to d.d.coren@sussex.ac.uk

[†] Now at the Whittle Laboratory, University of Cambridge

INTRODUCTION

This paper reports an experimental investigation into turbine stator well cavity cooling. Optimisation of the coolant and sealing flows in stator well cavities has potential benefits for both overall cycle efficiency and component life. As such, these themes provide the focus for the research here. In particular, the relationship between superposed cooling flow and rim seal ingestion, and the influence of coolant delivery geometry on cavity wall temperature distribution, is discussed here. Experimental findings are quantified in terms of a thermal effectiveness parameter, while CFD code has been used to reinforce understanding of the associated flow structures.

The flow and heat transfer within the cavities adjacent to the hub of a turbine stage has a significant effect on the durability of the neighbouring components. Stator well flows are characterised by regions of entrainment, cores of highly two dimensional rotationally dominated flow, and shear driven mixing regions both within the cavity and at the rim seals. Superposed cooling flows are required in order to ensure that engine components are kept within their rated working temperatures, either by direct cooling or by means of pressure sealing wheelspace and stator well cavities to avoid ingestion from the hot main gas path. These cooling flows influence the flow structures otherwise prevalent in rotor-stator cavities.

These phenomena represent the limits of Reynolds-Averaged Navier Stokes (RANS) approaches. More computationally expensive Large Eddy Simulation (LES) and hybrid techniques hold much promise, in particular for the prediction of mixing and interactions in the shear dominated regions. With the increased adoption of conjugate methods, the requirement for high quality validation data is clear.

Rig testing is often limited to a small number of geometrical variations before significant rebuild or re-instrumentation becomes necessary. The experimental data presented have been obtained using the Turbine Stator Well (TSW) test facility at the Thermo-Fluid Mechanics Research Center (TFMRC) at the University of Sussex. This facility is described in more detail by Coren *et al.* [1]. The Sussex Turbine Stator Well test rig comprises a two stage turbine with an overall pressure ratio of 2.7:1 at design conditions. It features an easily configurable working section which can be modified in a matter of hours. A brief overview of the test facility is given here, including description of the main annulus and internal cooling geometries, their control and supply system, and instrumentation specifications.

This work is part of the EU FP6 MAGPI (Main Annulus Gas Path Interactions) programme, which has the remit of improving current understanding of the interaction of cooling and main stream flows.

Since investigations related to the flows in the vicinity of turbine stator wells requires discussion of the flow physics associated with rotor-stator cavities, a brief review is included.

Rotor-Stator Flows

A disc rotating in the presence of a quiescent viscous fluid will entrain fluid and drive it radially outward in a three

dimensional viscous dominated boundary layer until it exits via the disc periphery. This is commonly referred to as the free disc case and provides useful reference for the study of rotating flows.

Daily and Nece [2] showed that for a rotor-stator arrangement with an aspect ratio, $G \leq 0.1$ and a circumferential sealing shroud, the working fluid recirculates around the cavity. Entrained flow pumped radially outward on the rotor surface is supplied by a radial inflow along the stator wall. These viscous boundary layer flows are separated by a two dimensional core which behaves inviscidly, and in the absence of circumferentially periodic protrusions, rotates at $\beta \approx 0.4$.

The rate at which the inviscid core rotates is a result of the rotor and stator boundary layers which form a viscous coupling and transmit a retarding force between the rotor and the stator. This was investigated by Owen and Rogers [3] who used a momentum integral approach to analyse this effect. The resultant relative tangential velocities that exist between the wall surfaces and the rotating core are proportional to the rate of frictional heating that occurs, which was investigated experimentally by Coren *et al.* [4].

The rate of entrainment for a free disc is given by the relation of Dorfman [5] for turbulent flow, Equation 1, while entrainment for partial rotors, as commonly found in turbomachinery, may be related to this by the fit of Chew [6], Equation 2.

$$C_{w,0} = 0.219 R e_{\phi}^{0.8} \quad \text{Equation 1}$$

$$C_{w,ent} = C_{w,0} \left[1 - \left[\frac{a}{b} \right]^5 \right] \quad \text{Equation 2}$$

Where: $C_{w,ent}$ = Flow entrained by a disc with inner hub

$C_{w,0}$ = Flow entrained by a free disc

and a and b are the inner and outer disc radii

The importance of accounting for disc pumped flow physics when modelling rotor-stator flows was demonstrated by Da Soghe *et al.* [7] who developed a design tool for solving steady one dimensional axisymmetric rotating cavity flows. The solutions predicted by the model were seen to more closely match experimental data and CFD predictions after developing correlations for disc friction.

Superposed Cooling Flows

Superposed cooling flows are required in order to provide direct cooling of critically loaded turbine components and to prevent bulk rim seal ingestion by pressure sealing the hub region cavities and wheelspaces from the hot gas path.

The minimum superposed throughflow required to achieve cavity sealing and avoid ingestion from the hot mainstream gas path may be estimated using correlations such as that of Owen

and Phadke [8]. The correlation of Owen and Rogers [3] provides such relation while accounting for circumferential pressure gradients in the main annulus, which were shown by Bunker *et al.* [9] to strongly influence rim seal flow exchanges. This was also investigated by Dixon *et al.* [10] using CFD.

The superposed cooling rate required for cavity sealing is generally found to exceed the entrainment rate. Such rates of superposed flow alter cavity flow structures strongly. The flow regime may be conveniently evaluated using a non-dimensional relation. The following is appropriate for turbulent flow:

$$\lambda_T = C_w Re_\phi^{-0.8} \quad \text{Equation 3}$$

The entrainment capacity of the rotating disc is exceeded when $\lambda_T \geq 0.219$, and radially dominated flow prevails. For values below this, flow may be considered to be rotationally dominated.

Daily *et al.* [11] related the rate of superposed cooling flow and the resulting core rate, β , to the core rate in the absence of superposed flow, β^* . Gartner [12] showed similarly that the presence of a two dimensional core was diminished as superposed flow was increased beyond the rate of disc entrainment. For these investigations, coolant was supplied axially from a non rotating source, such that increased coolant flow reduced core rates, ultimately flooding them with radial outflow dominated flow until free disc like flow structures and moment coefficients occurred.

However, as applied to the case of turbine stator well cooling where the coolant is supplied from a hub mounted passage rotating at rotor rate, a radial outflow, where relative tangential velocities across the rotor boundary layer are reduced is of benefit; after consideration for the work required to bring the coolant up to rotor rotational rates via pre-swirl nozzles incorporated into a rotating hub, as investigated by Karabay *et al.* [13], the relationship between cooling flow and the core rate becomes advantageous. This was demonstrated by Andreini *et al.* [14] who performed CFD analysis to investigate the effect of angled coolant passages.

Seal Flows

In an idealised environment, cavity flows would be isolated from the main annulus. In practice, high speed rotor-stator systems employ non-contact seals with finite clearance. This is set as small as possible, while accounting for thermal and rotational loads throughout the engine duty cycle, chiefly in order to reduce the superposed coolant required to achieve cavity sealing.

Rim seal flows, in simplified terms, are affected by pressure gradients acting across them, the running clearance; and also circumferential pressure gradients in the main annulus, as described by Owen and Rogers [3] and Scanlon *et al.* [15]. Interstage labyrinth seals provide means of containing upstream cavity flows prior to them exiting via either the rim or interstage seals themselves. Interstage seal flow rates are

dominated by the main annulus stage pressure drop and the effective area of the seal. Flow rates through rotor-stator labyrinth seals have been the attention of many studies, including that of Wittig *et al.* [16] who provided empirical correlation of seal geometries to standard seal flow equations, and Kim and Cha [17] who used the experimental data of Wittig to validate CFD models for rotating seal geometries.

Summary

Designing for cooling system effectiveness requires accurate prediction of the ingress and egress regime limits. For a given application, this requires consideration for superposed cooling flows, entrainment flows, interstage seal flows, and estimates of the minimum coolant required for cavity sealing. These flows are depicted, in simplified form in Fig. 1.

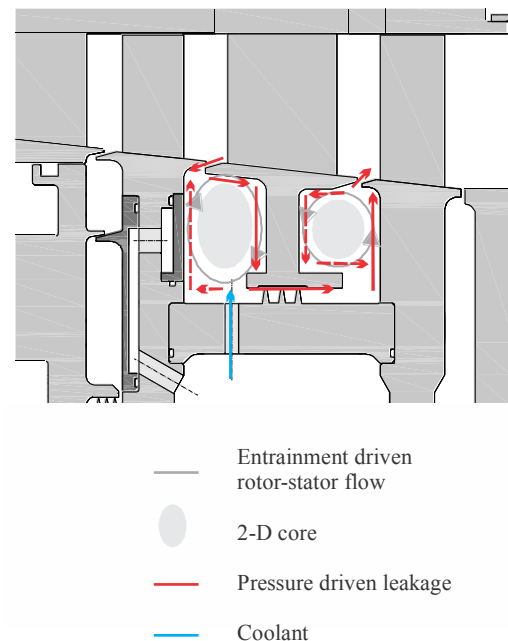


Figure 1: Rotor-Stator Flow Structure Schematic

In response, this paper presents data resulting from investigations carried out to determine the influence of the following cooling flow parameters; flow rate, cooling jet momentum, and flow trajectory. The experimental facility allows:

Coolant flow rates to be set below the disc entrainment and interstage seal demand to allow bulk ingestion, or set sufficiently high as to flood and seal the cavity to allow bulk egress.

The effective flow area of the coolant delivery passages to be altered such that, for a given rate of coolant, the momentum with which the flow enters the stator well cavity is increased, influencing cavity flow paths.

The use of angled coolant delivery passages, in order to impart the coolant flow with a particular trajectory, with the aim of improving the cooling of targeted components.

TEST FACILITY OVERVIEW

The test facility features a bespoke two stage turbine rated at 400 kW with blade geometry representative of modern gas turbines. A diagram of the test rig is given in Fig. 2. The rotor stages have 78 blades and the stators 39, which gives a convenient 2:1 repeat ratio for CFD.

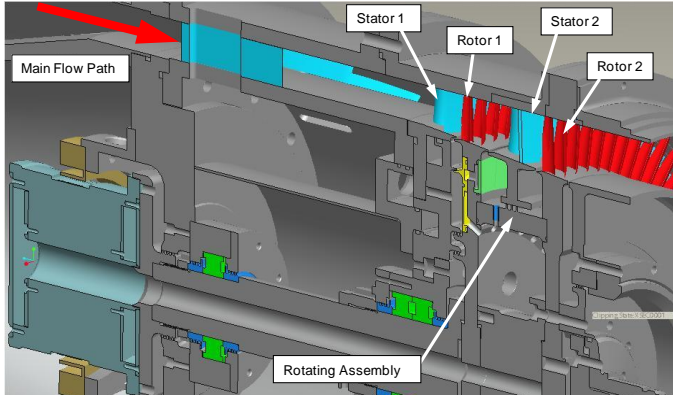


Figure 2: Schematic of the Test Rig Working Section

The main annulus flow is provided by an adapted aero engine plant driven compressor as developed by Turner *et al.* [18]. Flow enters the test rig via a settling chamber and large bellmouth inlet to reduce circumferential non-uniformity and swirl. The mass flow rate is measured using a BS1042 standard venturi meter. The turbine power is absorbed by a hydraulic dynamometer via a 3:1 reduction gearbox. The main annulus operating conditions are given in Table 1.

Overall Pressure Ratio	< 2.7
Power Output	< 400 kW
Mass flow rate	1 to 4.8 kgs ⁻¹
Cooling flow rate	0.6 to 1.65 $C_{w,ent}$
T_{inlet}	300 – 450 K
P_{inlet}	< 3.3 bar
N (at design condition)	10,630 rpm

Table 1: Test Rig Main Annulus Operating Conditions

Of central importance to the design of the test rig is the ability to readily reconfigure the cooling system geometry. This is provided by a split main casing design which allows rapid access to the stator well cavities.

Internal Air System

The stator well cavity geometry has been designed to provide a nominal in-cavity Reynolds number of $Re_{\phi} = 2.0 \times 10^6$ at the main annulus design condition. Cooling flow rates have been specified to encompass the ingestion point, the selection process having been informed by a review of cavity sealing correlations. The maximum rate of superposed cooling flow allows the equivalent of 2.8 greater than the minimum suggested for cavity sealing by the correlations of Owen and Phadke [8]. The interstage labyrinth seal geometry has been set such that the seal flow may be exceeded by superposed cooling

flow, allowing cavity flow conditions to be controlled by superposed coolant. The maximum cooling flow rate is equivalent to 1.8 times the interstage labyrinth seal flow requirement as predicted using the correlation of Wittig *et al.* [16] and the study of Kim and Cha [17]. This particular aspect of this work is presented in more detail by Eastwood *et al.* [19]. Taken together, this allows interstage seal demand to be satisfied and rim sealing to be achieved, with a safety factor included to account for the variation between the correlations used. Importantly, this allows cavity flow conditions from bulk ingestion to bulk egress to be tested.

Non-dimensioning of the superposed cooling flow is useful in widening the range of applicability of the results obtained. The rate may be related to the minimum required to seal the cavity, or to the interstage seal demand, using one of the many correlations available from the literature. However, there is much variation between the results of these correlations, indeed this present work seeks to further clarify the conditions required for cavity sealing. Also, the interaction of superposed coolant with entrainment flows is of particular interest to this study. For these reasons, the superposed coolant has been defined here in terms of a disc entrainment parameter, using Equations 1 and 2. The data presented here relates to experiments where cooling flow is delivered in a variety of manners. Each of these different test cases results in a unique value of core rotation rate, β . As such, the free disc case, modified using Equation 2 to account for the partial disc geometry in question, is considered to provide a non-ambiguous bench marked reference case, to which the superposed coolant rates may be equated to. The cooling system has been specified to allow coolant flow, $C_{w,s}$ over the range 0.60 to 1.65 times the predicted disc entrainment, $C_{w,ent}$. For the cooling flow data presented here, rates of 0.71, 0.87, 1.13 and 1.46 $C_{w,ent}$ have been used, which accounts for augmentation due to balance seal leakage flows.

The cooling system air is supplied by an Atlas Copco ZT250 compressor and FD710 drier plant. The test rig internal air flow circuits are shown in Fig. 3. The cooling system air is ducted via aerodynamic struts into the hub region of the rig, similar ducting is used for the balance and vent flows. Coolant is delivered to the cavity first via transfer holes in the lower part of Stator 1, and then via transfer holes in the hub region of Rotor 1. A pressure balanced, double sided claw seal is used to reduced leakage of coolant flow up through the Stator 1 wheelspace. The balance cavity is continuously monitored during tests to account for thermal growth of the claw seals. The balance supply is vented from a buffer cavity to maintain upstream wheelspace egress. Although the rig design permits both radial and axial delivery of coolant, radially administered coolant is the focus of this paper. The radial coolant passage design features 39 threaded holes equi-spaced around a hub ring, into which inserts drilled to form coolant passages may be installed. The air paths are insulated from the main annulus temperatures by Rohacell HF insulation. Bosch HFM 5 series hot-film air mass meters are used to measure the coolant, wheelspace balance and vent flows. They operate over the

range 0 to 100 gs^{-1} and were calibrated by a UKAS accredited third party. They give an uncertainty of $\pm 1.3\%$ of the measurement point.



Figure 3: Internal Air System Schematic

The influence of cooling flow jet momentum is facilitated by varying the number of drilled and blank radial flow passage inserts, as shown in Fig. 4. This arrangement allows 13, 26 or 39 coolant passages to be incorporated, providing means to alter the momentum of a given rate of exiting coolant by a factor of three. Removable cover plates on the downstream face of Rotor 1 allow axially delivered coolant to be similarly regulated. Regular spacing in all cases discourages non-axisymmetric cooling effects and simplifies balancing of the rotating assembly.

Description	Geometry
39 Radial Passage Inserts	
26 Radial Passage Inserts	
13 Radial Passage Inserts	

Figure 4: Radial Flow Passage Spacing Arrangements

The influence of coolant trajectory is facilitated by means of angled coolant delivery inserts, as shown in Fig. 5. Using delivery passages with an angle from a reference straight radial

outlet, the coolant may be imposed to follow a trajectory directed either axially towards the rotor face to encourage attachment with entrainment flows, or tangentially to pre-swirl the coolant against the direction of core rotation slippage. For the purposes of this study, axially directed coolant is considered. An angle of 25° has been used, which was informed by design phase CFD.

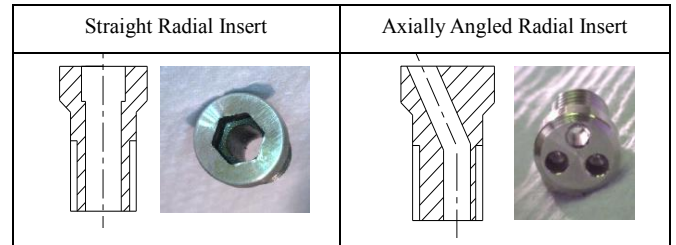


Figure 5: Straight and Axially Angled Radial Flow Passage Inserts

Ensuring that the inserts are installed with the angled passage aligned in the correct direction is performed by means of bespoke alignment jigs. Through this process, a maximum angular deviation of 0.3° is achieved.

Temperature Instrumentation

The measurement locations of the thermocouples within the main test section of the rig are given in Fig. 6. In total, 81 K-type thermocouples at 27 radial locations have been installed within the rotating assembly, including two air thermocouples used for coolant temperature measurements. 73 thermocouple measurement locations were used within the stationary components of the test rig, six of which are stator mounted air thermocouples. Total temperature measurements are made in the main annulus using probes set into the leading edge of Stator 1, Stator 2 and with a radial rake downstream of Rotor 2. This avoids the introduction of additional disturbances to the circumferential pressure gradients at the rim seal region.



Figure 6: Temperature Measurement Locations

Three thermocouples were used for each radial measurement location on the rotating components to mitigate thermocouple failures. In practice, a thermocouple mortality rate of 8% has been found.

The thermocouple beads, with diameters ≤ 0.1 mm, are peened into the material surface as shown in Fig. 7. The lead-out trails, which are led at least 10 diameters circumferentially before radially to avoid conduction errors, are secured to the rotating components by means of spot welded metallic straps. Peening with similar material, and flush mounting to minimise velocity effects, helps to reduce embedding errors.



Figure 7: Thermocouple Installation Detail

A Datatel 92 channel telemetry system is used for thermocouple signal acquisition. Each unit has an in house cold junction reference module with a PRT mounted in close thermal contact to thermocouple junctions. For a given test the point to point resolution appears to be within 0.1 K. Comprehensive through-calibration techniques have reduced uncertainties to the order of 0.3 K across a 12 month period.

The stationary frame thermocouples are installed without the use of extension cables or plugs, directly into isothermal junction boxes with thick copper heat spreaders which have been fitted with PRT thermometers. These are logged using an Agilent 34970a DVM switch unit in 4-wire resistance mode. Combined with full through-calibration techniques, this reduces cold junction compensation errors to within 0.1 K.

All through-calibration is performed by comparison against Isotech Secondary Standard reference equipment with a combined uncertainty in the region of 20 mK. The test data described here have been obtained at settled conditions, defined as a change of less than 0.1 K over a five minute period.

In the interests of allowing cross comparison of test data, where small variations in main annulus and environmental conditions may be unavoidable, it is convenient to express temperature data in a normalised form;

$$\theta = \frac{T_{metal} - T_{cold}}{T_{hot} - T_{cold}} \quad \text{Equation 4}$$

This method is, however, classically ill conditioned and provides motivation for obtaining very low temperature measurement uncertainties. When the metal temperature, T_{metal} , and coolant temperature, T_{cold} , are similar, as is the case at the lower regions of the cavity, small errors will dominate. For example, a temperature difference of 10 K would yield a potential uncertainty of $\pm 3\%$ θ for an uncertainty of ± 0.3 K. Repeat testing over several months showed repeatability in normalised temperatures of approximately 1% at worst; within measurement uncertainty, suggesting that the calibration uncertainties quoted are realistic under actual test conditions.

Pressure Instrumentation

The location of the pressure measurements within the main test section of the rig are shown in Fig. 8. These are used to determine the conditions in the stator well cavities, to measure flow rates of air supplied to the rig, and to allow balancing of the upstream wheel space. Total pressure measurements are made in the main annulus using probes set into the leading edge of the NGVs. The incidence sensitivity of the total pressure measurements is minimised by recessing the tapings. All internal rig measurements use Scanivalve DSA 3217 scanner units. The orifice plate measurements use Rosemount 1151 series (differential) and Mensor 6100 (absolute) transducers.

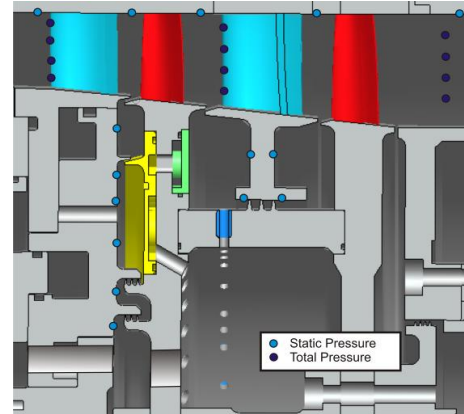


Figure 8: Pressure Measurement Locations

VISUALISATION CFD SET-UP AND ANALYSIS

The CFD analysis presented here is adiabatic and intended for flow visualisation purposes; stator well cavity streamlines representing the flow structures associated with particular cooling flow cases provide a useful aid in interpreting the measured temperature data. The domain was split into four zones separated by mixing planes between the blade rows, and an interpolation, or frozen sliding plane, between the upstream and downstream cavities. These are illustrated in Fig. 9.

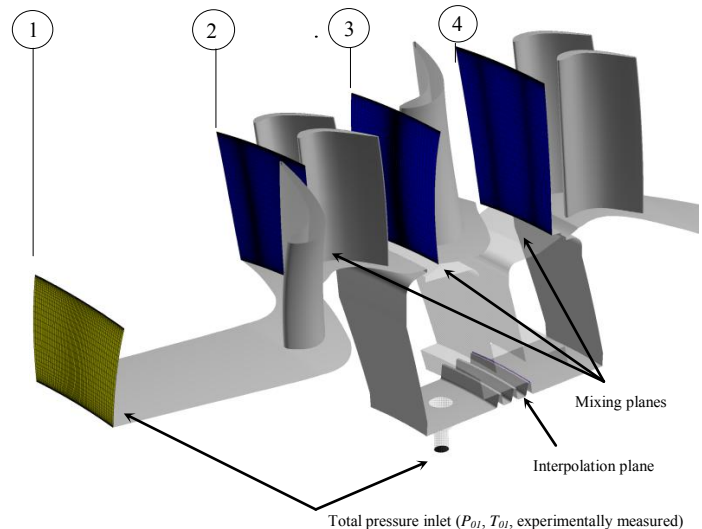


Figure 9: CFD Domain Showing Thermodynamic Stations

The multi-block structured mesh was generated using the Rolls-Royce PADRAM code and features nine Million nodes. The grid density is biased somewhat towards the cavity. The mixing plane upstream of Stator 2 is set well beyond the stationary side of the rim seal in order to model the unsteady, albeit frozen, rotor exit flow field. Grid dependency, and the effect of unsteadiness is presented by Dixon *et al.* [10].

Measured total pressure and temperature boundary conditions were used at stage inlet, and measured static pressure at the stage outlet. For the radial coolant injection, the mass flow rate is measured, but the actual total pressure is unknown.

Rim seal flows are unsteady in nature, however the unsteadiness is only likely to be dominant at the point at which the cavity is almost sealed. The steady computations presented here represent several months of computational time on a 64 CPU cluster. This work is part of an on-going study, the primary aim of which is to help validate Conjugate Heat Transfer (CHT) methods. The added fidelity of the unsteady model is considered less important than some of the other simplifications such as the use of an adiabatic solution. The steady state convergence showed oscillatory behaviour at the low coolant flow rates. The rim seal interactions are dominated by the unsteady Kelvin-Helmholtz (K-H) type interactions and the potential field of the rotor, as such the exact sealing boundary is not expected to be predicted. Also the Reynolds Averaged Navier-Stokes (RANS) approach is not well suited to the mixing and ingestion anyway. The computations are presented here simply to aid understanding of the flow.

In order to establish confidence in the cavity CFD, main annulus and interstage labyrinth seal flows have also been modelled, and are described in this section below.

Main Annulus Flow

A comparison of the predicted and total pressure and temperature at 4 discreet locations on the Stator 2 leading edge is shown in Fig. 10. Data is presented for an intermediate coolant flow test case. The plot shows total temperature T_{03} , normalised by the inlet total temperature T_{01} and total pressure P_{01} respectively, i.e. the inlet boundary conditions. The agreement at the middle two measurement locations is excellent. The worst case absolute temperature difference is ± 0.5 K for a stage temperature drop of ~ 50 K; this represents a fair comparison rather than the simple Kelvin value which would simply hide the variations. This is close to the combined measurement uncertainty of ± 0.3 K. The total pressure values at the three upper locations are within 0.2 % of the measured value. These two middle locations are away from the majority of the loss and secondary flow structures. As such the close agreement of the values suggests that the overall operation of the stage is well modelled by the grid.

At the upper and lower radial heights the CFD solution over-predicts the total temperature and pressure. At the upper radial location, the total temperature discrepancy is ~ 3 K, which represents 6 % of the stage total temperature drop. At the

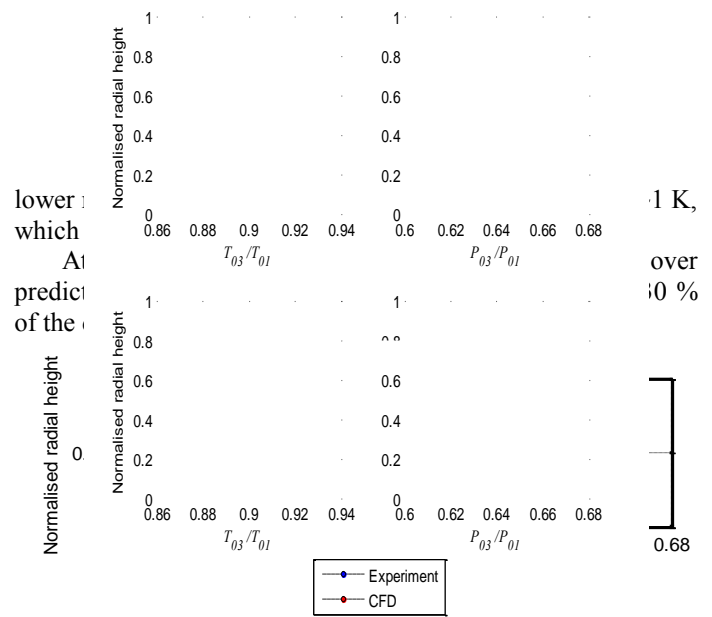


Figure 10: Comparison of predicted total pressure and temperature at the inlet to Stator 2

An area traverse of predicted total pressure and temperature ratio corresponding to a location close to the leading edge of Stator 2, but upstream of the mixing plane, is shown in Fig. 11.

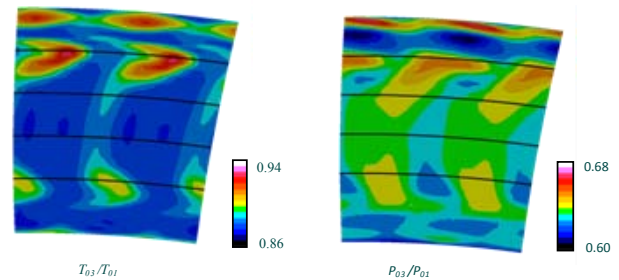


Figure 11: Total Pressure and Temperature Profiles at the Stator 2 Leading Edge Plane

The upper and lower radial heights correspond to the height at which the secondary flow structures impinge on the leading edge of the vane. As such, it is expected that the discrepancy is primarily due to the prediction of the secondary flows. The main stream grid is perhaps a little coarse, the use of a mixing plane removes all of the rotor-stator interactions, and the limitation of the Spalart-Allmaras (S-A) turbulence model to predict the mixing accurately are all likely to be significant. It should also be noted that there are steep gradients at these locations, so the predictions are also highly sensitive to the precise spatial location of the flow structures. The non-linear interactions of the upstream vane wake and vertical structures with the blade boundary layer and secondary flows are removed by the mixing plane. Blade row interactions of this type have been shown to account for 10 % of stage loss.

Another factor at the hub, where the discrepancy in total pressure is found, is the lack of the upstream wheel space cavity on the model. Although the egress is limited to approximately, 2 gs^{-1} , the presence of the cavity alone is likely to thicken the boundary layer at the very least.

These variations are local, and the excellent tie-up in the core flow shows that the model is adequate to generate the boundary conditions at the rim seal.

Interstage Labyrinth Seal Flow

Numerous articles have been published on labyrinth seal flows. The seal flow is modelled here using the St. Venant-Wantzell equation for the ideal flow together with a single discharge coefficient, C_D , which accounts for all of the dependent parameters. The discharge coefficient, C_D , for the seal is a strong function of clearance.

The TSW interstage labyrinth seal is a three fin straight through seal with a cold build clearance of 0.3 mm, which grows by approximately 30 % at the design condition. This has been set so that the seal demand is of a similar order to disc entrainment flow and also the superposed coolant, when $C_{w,s}$ is approximately $0.7 C_{w,ent}$. At the design condition, the throughflow Reynolds number, Re_z is in the order of 7×10^3 , and the ratio of axial to tangential velocity is approximately unity. For the purpose of this work, an initial flow estimate has been established using the two-dimensional, non-rotating data of Wittig *et al.* [16]. These authors considered the effects of rotation to be dominant only at low Reynolds numbers. An estimate for the three fin C_D was derived from the numerical modelling of the Wittig *et al.* data by Kim and Cha [17]. Based on their results, a C_D estimate of 0.48 has been used here.

The CFD results have been compared with results from labyrinth seal flow models, using pressure ratios representative of the experimental conditions tested. Agreement was found to be within the range 0.5 to 2 % as the pressure ratio was increased. These seal flows provide the focus of the work described by Eastwood *et al.* [19].

RESULTS AND DISCUSSION

The cooling effectiveness associated with cooling flow; rate, momentum, and trajectory are discussed here, in terms of temperature data obtained by experiment which has been normalised using Equation 4. The discussion is aided by either CFD results or flow diagrams.

The effect of core rotation rate is not included in the normalisation as the interaction of the coolant and the rotating core is a component of the performance of a particular cooling arrangement in itself, which is essentially part of this study.

As the coolant air temperature is measured at a lower radius than the cavity entry, the Euler work due to the change in radius is taken into account; ≤ 3 K for these cases, assuming the coolant enters and leaves the internal passage with little rotor relative swirl:

$$T_{0,cold} = T_{0,coolant} + \frac{1}{c_p} \Delta[(r\omega)^2] \quad \text{Equation 5}$$

Cooling Flow Rate

The effect of coolant flow rate is described here with the aid of both experimental data and CFD results for the case of 39 radial coolant delivery passages. Normalised measured metal temperatures are shown for the measurement locations on

the rear face of Rotor 1 in Fig. 12, and for the front face of Stator 2 in Fig. 13. Fig.14 shows the predicted path of main stream and coolant flow gas, for the two lowest coolant flow rates. The streamlines are seeded from the Rotor 1 aft platform boundary layer and the coolant supply jet respectively. Fig. 15 shows the rotor relative frame total temperature in the cavity at the four coolant flow rates. These figures may be used to help explain the temperature profiles observed in the measured data. The CFD predictions are used only to provide a qualitative prediction of the likely flow structure, in order to help interpret the measured profiles.

Referring to Fig. 12, it is important to note that at all four coolant flow rates the normalised temperature is approximately constant at the location on the Rotor 1 exit platform ($r/b = 1$) as would be expected. The temperature gradient between the two highest radius locations, $0.97 \leq r/b \leq 1$, is perhaps the most important part of the data set. Considering the titanium rotor, changes in temperature gradient at this location imply considerable changes in the local aerodynamic conditions, at least in terms of air temperature, if not heat transfer coefficient. At the lowest coolant flow rate, $0.71 C_{w,ent}$, there is little change in gradient across all three high radius positions shown. As the coolant flow rate is increased to $0.86 C_{w,ent}$, and $1.13 C_{w,ent}$, the gradient increases, indicating that the coolant is penetrating to higher radial locations in the cavity. This is in agreement with the CFD results in Fig. 15 which indicate significant change in cavity flows for superposed coolant rates of $\leq 0.86 C_{w,ent}$. A further increase in coolant flow rate from 1.13 to $1.46 C_{w,ent}$, yields a lower increase in temperature gradient. This indicates that the cavity is likely to be well sealed and the changes in cavity flow structure are small. At the lower extreme of the cavity, there is a larger variation in normalised temperature with coolant flow rate. This is likely to be driven by conduction, rather than differences in local adiabatic effectiveness, since this is in the vicinity of the coolant delivery passages. Even at the lowest coolant flow rate, the coolant will circulate in the lower extremes of the cavity. This is in agreement with the CFD for the low cooling flow case shown in Fig. 14. Although the spatial gradient is higher at the lower measurement points, $0.755 \leq r/b \leq 0.77$, than the outer two, $r/b = 0.97 \leq r/b \leq 1$, there is less *change* in gradient with increased coolant flow.

Referring to Fig. 13, an increase in the superposed cooling supply from $0.71 C_{w,ent}$ to $0.86 C_{w,ent}$ results in increased cooling at the cavity region of $0.77 \leq r/b \leq 0.945$. This is likely to be due to localised cooling of the stator foot as coolant enters the cavity. For the majority of the cavity, $0.78 \leq r/b \leq 0.99$, it is clear that the cavity is in contact with significant coolant between the supply conditions $0.71 C_{w,ent}$ and $0.86 C_{w,ent}$. This is in agreement with the CFD shown in Fig. 15. Increasing the coolant rate to $1.46 C_{w,ent}$ results in no significant additional cooling at these locations. However, at the outer most radial location, $r/b = 0.99$, which is in the main annulus, normalised temperatures can be seen to be reduced significantly at cooling rates of $\leq 1.13 C_{w,ent}$, indicating that rates sufficient for cavity sealing and bulk egress have been reached. This is in agreement with the CFD for higher coolant rates shown in Fig. 15.

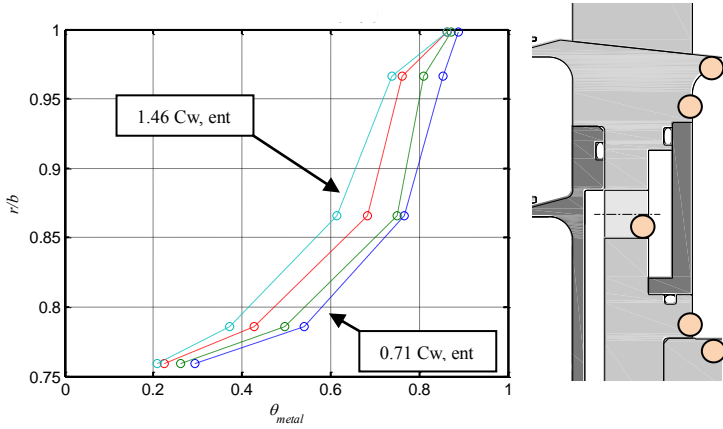


Figure 12: Rotor 1 Rear Face Normalised Metal Surface Temperatures

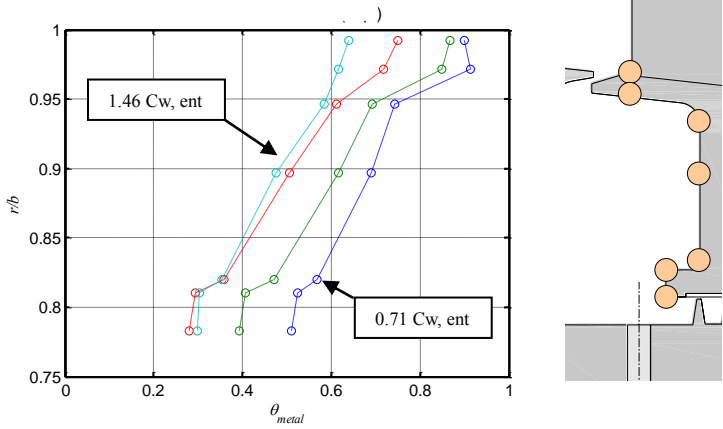


Figure 13: Stator 2 Front Face Normalised Metal Surface Temperatures

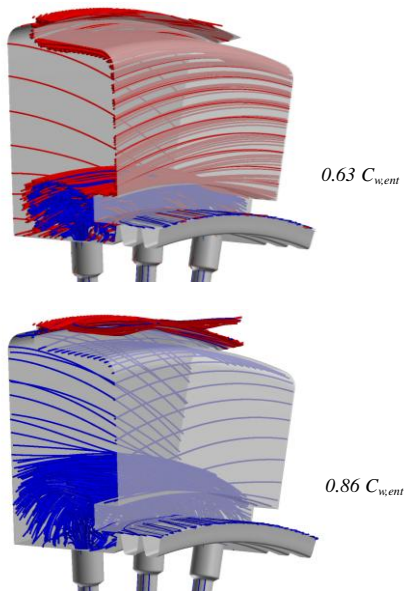
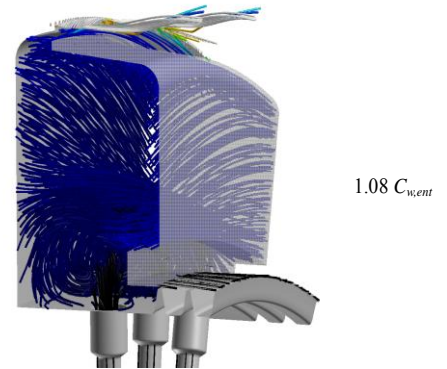
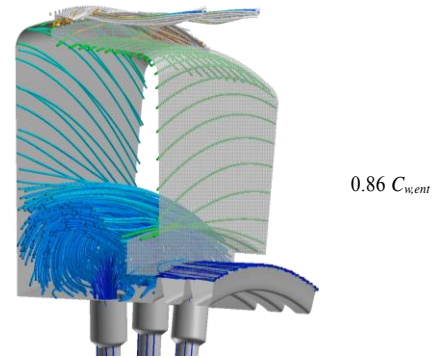
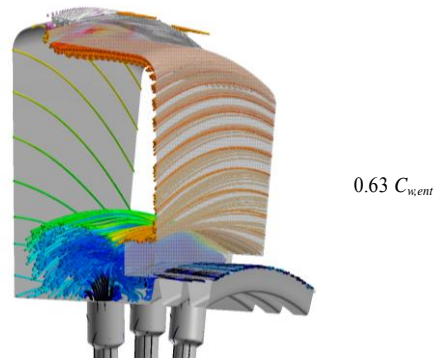


Figure 14: Comparison of Predicted Coolant (Blue) and Mainstream (Red) Streamlines.



T_{cold} T_{hot}

Figure 15: Cavity Streamlines, Coloured by Normalised Absolute Frame Total Temperature

Jet Momentum

Deeper penetration of the coolant streams into the cavity bears influence on the rate of core flow rotation, reducing the relative tangential velocity across the rotor boundary layers. Furthermore, for the split stator well cavities being considered here, deeper penetration encourages coolant to feed the Rotor 1 entrainment flow rather than exit through the interstage seal to the downstream cavity. This was found to be particularly evident at low cooling flow rates. Since mass flow is constant and internal cooling effects may be largely neglected, axial as well as radial delivery geometry data are considered here.

Fig. 16 shows results obtained for the downstream face of Rotor 1 in the form of normalised temperatures at a cooling flow of approximately $0.7 C_{w,ent}$ delivered radially. Reducing the effective flow area, by reducing the number of flow passages from 39 to 13, increases jet momentum threefold thereby increasing coolant flow impingement into the stator well cavity. Normalised temperatures are reduced in the vicinity of the hub region by up to 50 %, and in the region of the rotor periphery by approximately 20 %.

Measurements for the upstream face of Rotor 2 are shown in Fig. 17. In the downstream cavity, the influence of jet momentum is diluted, since the cooling air will already have mixed with ingested gas in the upstream cavity. However, as the number of flow passages is increased to 39, normalised temperatures do decrease, suggesting that cooling effectiveness has increased. This is likely to be related to the amount of heat absorbed by the coolant in the upstream cavity prior to flowing through the interstage seal.

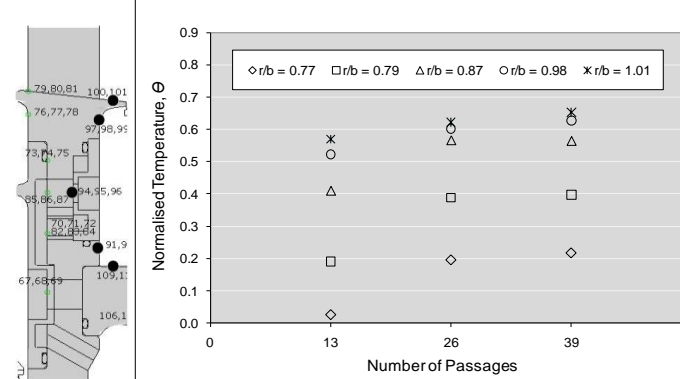


Figure 16: Rotor 1, $0.7 C_{w,ent}$, Radial Delivery

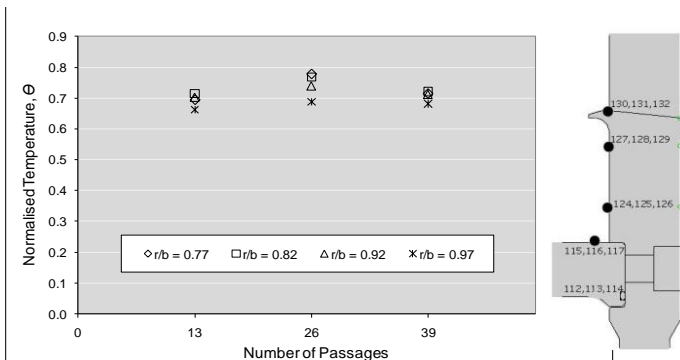


Figure 17: Rotor 2, $0.7 C_{w,ent}$, Radial Delivery

It is interesting to note that at these conditions, the reduced adiabatic viscous heating corresponding to an arbitrary change in β from 0.5 to 0.7 would equate to a 15 % reduction in the normalised measured temperatures at the rotor periphery. This equates to approximately 50 % of the total measured change between 39 and 13 coolant passages, suggesting that the temperatures measured are a result of core rate change but also re-distribution of the coolant.

Adiabatic flow visualisation CFD in Fig. 18 shows coolant delivered radially through 39 and 13 holes at $0.7 C_{w,ent}$. Streamlines indicate that the level of cavity impingement increases significantly as the number of flow passages is reduced from 39 to 13. This is likely to result in greater attachment to Rotor 1 entrainment flows, and strongly reinforces the interpretation of the experimental data.

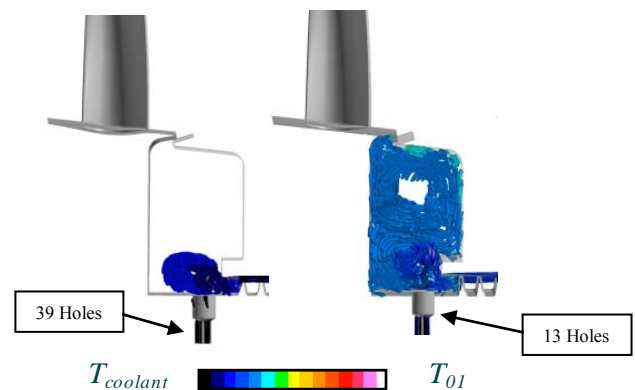


Figure 18: CFD Showing Cavity Impingement Increasing as Radial Flow Passage Number is Reduced from 39 to 13 at $0.63 C_{w,ent}$

Data also obtained at a cooling flow rate of $0.7 C_{w,ent}$ but for axially delivered coolant shows broadly similar results. See Fig. 19. Reduced benefit at the cavity periphery, as compared to the radial geometry, is considered to be a generic characteristic of axial delivery passage geometry, which supplies coolant to this region for all momentum cases. Increased cooling at the hub region for the 13 passage case may be a result of recirculation local to the rotor face.

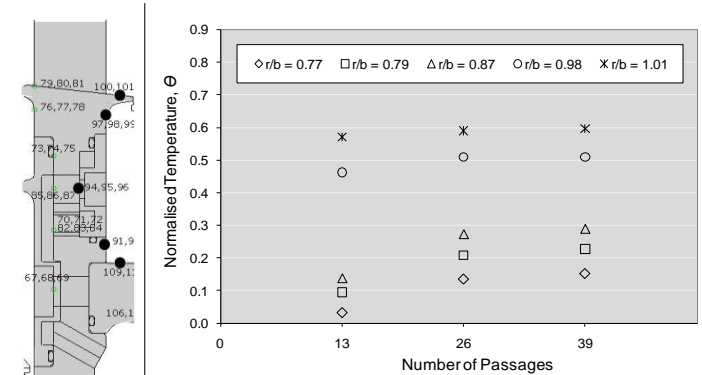


Figure 19: Rotor 1, $0.7 C_{w,ent}$, Axial Delivery

At the higher cooling flow rates of 1.13 and 1.46 $C_{w,ent}$, tested for 26 and 39 passage geometries only, the cavity flows are dominated by the sheer magnitude of coolant flooding

cavity and the influence of jet momentum is less obvious. This is demonstrated in Fig. 20 by data obtained for radially delivered flow at $1.46 C_{w,ent}$.

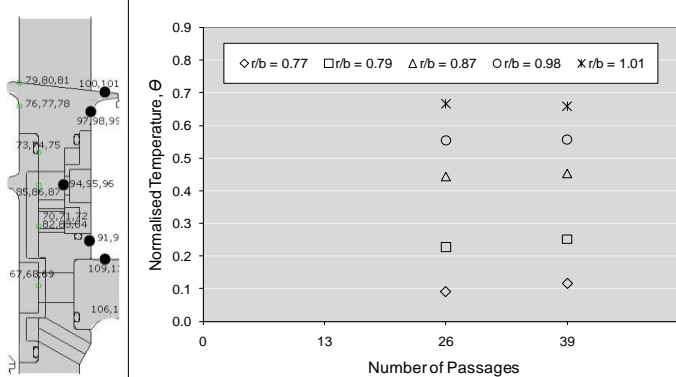


Figure 20: Rotor 1, $1.46 C_{w,ent}$ Radial Delivery

Angled Delivery Geometry

The angled insert design incorporates a flow passage inclined at 25° . This value was selected after an optimisation process involving design phase CFD investigations, which have been reported by Andreini *et al.* [14] and also a result of the angle and bore size permitted by the insert location drillings. Settled data obtained at 9800 rev/min, and also data obtained during commissioning tests at the design condition but not as well settled, have all shown improved cooling effectiveness on Rotor 1 at the cavity periphery.

Normalised temperature data for the downstream face of Rotor 1, and also for the upstream face of Rotor 2, is shown for both straight and axially angled radial insert geometries in Fig. 21. This data was obtained at a superposed cooling rate of $0.86 C_{w,ent}$. A flow schematic is also given, aiding the description of the altered flow structures associated with the geometry changes. The change in the radial temperature profiles between the results for the straight and angled geometries suggests that the coolant has successfully been re-directed; increasing the likely-hood of attachment to the rotor entrainment flows, rather than washing over the stator wall or exiting directly through interstage seal into the downstream cavity. Similarly to the jet momentum experiments, even at low cooling flow rates, the hub region is subject to effective cooling, by virtue of proximity to the coolant delivery point; this is illustrated by the CFD results shown in Fig. 14. It is of particular interest to see that for this intermediate cooling condition of $0.86 C_{w,ent}$, with the introduction of an angled passage, cooling is re-directed to the cavity periphery significantly enough to result in a 10 % reduction in the normalised rotor temperature. The likely transit mechanism for this re-distribution is carriage within the disc entrainment flows. Corroborating this, the stator temperatures, while also reduced at the cavity periphery, are actually increased at the lower radii, indicative of re-circulated coolant which has been subject to heat pick-up.

The reduction in adiabatic viscous heating corresponding to an arbitrary change in β from 0.5 to 0.7 would equate to approximately 70 % of the measured change in normalised

temperature, suggesting that the reduced temperatures are strongly related to the core rate change, but also a result of re-distribution of coolant.

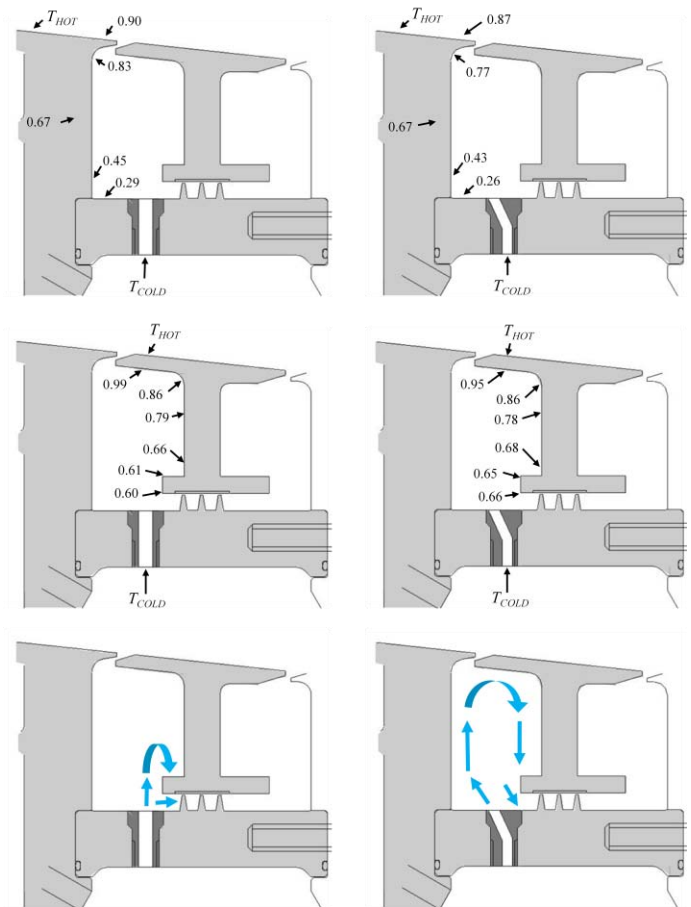


Figure 21: Normalised Temperature Data and Flow Structure Schematics for Straight and Axially Angled Radial Coolant Delivery, $0.86 C_{w,ent}$.

CONCLUSIONS

Developing an effective cooling system, where bulk ingestion is prevented and critical components are adequately cooled, requires a design process informed by the geometric characteristics and the associated flow physics of the target application. This approach, where the ingestion point is identified as a result of considering the interaction of the cavity flows, is essential in the quest to develop competitive engines.

Normalised temperature data presented in this paper demonstrate that the ingestion region for turbine stator wells may be identified with respect to disc entrainment parameters when considered in conjunction with visualisation CFD and understanding of the flow physics present.

It has been shown that the relative tangential velocities, and associated heating, that the highly stressed rotor is subjected to may be reduced by employing cooling path geometry that provides increased coolant delivery momentum. It has also been shown that, by taking advantage of already present entrainment flows, the trajectory of superposed cooling

flows may be specified to deliver coolant to preferred locations by means of angled coolant passage geometry features. Both approaches have been demonstrated to improve cooling effectiveness for a given rate of coolant.

The rotor-stator cavities found in gas turbines are home to complex and composite flows during engine operation. The findings presented here demonstrate that improvements in cooling system design may be found by analysing and exploiting these flows.

ACKNOWLEDGMENTS

The authors would like to thank Rolls-Royce plc for their support and permission to publish this work. Particular thanks are also given to Simon Davies, James Turner, and Tim Scanlon for their assistance in developing the facility. The present investigations were supported by the European Commission within the Framework 6 Programme, Research Project 'Main Annulus Gas Path Interactions (MAGPI), AST5-CT-2006-030874. This financial support is gratefully acknowledged.

REFERENCES

- [1] Coren, D. D., Atkins, N. R., Turner, J. R., Eastwood, D., Davies, S. Childs, P. R. N., Dixon, J. A., Scanlon, T. S., 2010, "An Advanced Multi-Configuration Stator Well Cooling Test Facility", Proceedings of ASME Turbo Expo 2010, Paper Number GT2010-23450
- [2] Daily, J. W., Nece, R. E., 1960, "Chamber Dimension Effects on Induced Flow and Frictional Resistance of Enclosed Rotating Discs", Journal of basic engineering, Vol.82., pp.217-232.
- [3] Owen, J. M., Rogers, R. H., 1989, "Flow and Heat Transfer in Rotating-Disc Systems: Volume 1 - Rotor-Stator Systems", Research Studies Press, John Wiley and Sons
- [4] Coren, D. D., Childs, P. R. N., Long, C. A., 2009, "Windage Sources in Smooth-walled Rotating Disc Systems", Proc. IMechE Vol.223, pp. 873-888, Part C: J. Mechanical Engineering Science.
- [5] Dorfman, L. A., 1963, "Hydrodynamic resistance and the heat loss of rotating solids", Oliver & Boyd.
- [6] Chew, J.W., 1998, "The Effect of Hub Radius on the Flow Due to a Rotating Disc", Journal of Turbomachinery, Vol. 110, pp.417-418.
- [7] Da Soghe, R., Facchini, B., Innocenti, L., Micio, M., 2009, "Analysis of Gas Turbine Rotating Cavities by a One-Dimensional Model", Proceedings of ASME Turbo Expo 2009, Paper number GT2009-59185.
- [8] Owen, J. M., Phadke, U. K., 1980, "An Investigation of Ingress for a Simple Shrouded Rotating Disc System with a Radial Outflow of Coolant", ASME Paper 80-GT49, 1980.
- [9] Bunker, R. S., Laskowski, G. M., Bailey, J. C., Palafox, P., Kapetanovic, S., Itzel, G. M., Sullivan, M. A., Farrell T. R., "An Investigation of Turbine Wheel-space Cooling Flow Interactions with a Transonic Hot Gas Path - Part 1: Experimental Measurements", 2009, Proceedings of ASME Turbo Expo 2009, Paper number GT2009-59237.
- [10] Dixon, J. A., Brunton, I. L., Scanlon, T. J., Wojciechowski, G., Stefanis, V., Childs, P. R. N., 2006, "Turbine stator well heat transfer and cooling flow optimisation", ASME paper GT2006-90306.
- [11] Daily, J. W., Ernst, W. D., and Asbedian, V. V., 1964, "Enclosed Rotating Disks with Superposed Throughflow", Dept. of Civil Engineering, MIT, Report No.64.
- [12] Gartner, W., 1997, "A Prediction Method for the Frictional Torque of a Rotating Disc in a Stationary Housing with Superimposed Radial Outflow", ASME paper, 97-GT-204.
- [13] Karabay, H., Pilbrow, R., Wilson, M., Owen, J. M., "Performance of Pre-Swirl Rotating-Disc Systems", ASME paper, 99-GT-197.
- [14] Andreini, A., Da Soghe, R., Facchini, B., "Turbine Stator Well CFD Studies: Effects of Coolant Supply Geometry on Cavity Sealing Performance", Proceedings of ASME Turbo Expo 2009, Paper number GT2009-59186.
- [15] Scanlon, T., Wilkes, J., Bohn, D., Gentilhomme, O., 2004, "A simple method for estimating ingestion of annulus gas into a turbine rotor stator cavity in the presence of external pressure variations", ASME paper GT2004-53097.
- [16] S. Wittig, U. Schelling, S. Kim, and K. Jacobsen, 1987, "Numerical predictions and measurements of discharge coefficients in labyrinth seals", ASME, International Gas Turbine Conference and Exhibition, 32nd, Anaheim, CA, 1987, p. 1987.
- [17] Kim, T. S., Cha, K. S., 2009, "Comparative analysis of the influence of labyrinth seal configuration on leakage behaviour", Journal of Mechanical Science and Technology 23 (2009) 2830~2838.
- [18] Turner, A. B., Davies, S. J., Childs, P. R. N., Harvey, C.G., Millward, J. A., 2000, "Development of a Novel Gas Turbine Driven Centrifugal Compressor", Proc. Instn. Mech. Engrs. Vol. 214, Part A, pp. 423-437.
- [19] Eastwood, D., Coren, D. D., Long, C. A., Atkins, N. R., Turner, J. R., Childs, P. R. N., Scanlon, T. S., Guijarro-Valencia, A., 2011, "An Experimental Investigation of Turbine Stator Well Rim Seal, Re-Ingestion and Inter-Stage Seal Flows Using Gas Concentration Techniques and Displacement Measurements", Proceedings of ASME Turbo Expo 2011, Paper Number GT2011-45874.